Desalination and Water Treatment 318 (2024) 100402

Contents lists available at ScienceDirect

Desalination and Water Treatment

journal homepage: www.sciencedirect.com/journal/desalination-and-water-treatment/

Preparation of versatile polymer particles and their application for elimination of bromophenol blue and phenol from aqueous environment

Kutalmis Gokkus[a,*,1], Cigdem Oter[b,2], Merilyn Amlani[c], Mahmut Gur[d,3], Vural Butun[e,4]

[a] Kastamonu University, Faculty of Engineering and Architecture Department of Environmental Engineering, Kuzeykent Campus, 37500 Kastamonu, Turkey
[b] Van Yuzuncu Yil University, Faculty of Science, Department of Chemistry, Van, Turkey
[c] Mindanao State university, Tawi-Tawi College of Technology and Oceanography, 7500 Marawi, the Philippines
[d] Kastamonu University, Faculty of Forest Department of Forest Industrial Engineering, Kuzeykent Campus, 37500 Kastamonu, Turkey
[e] Osmangazi University, Faculty of Science, Department of Chemistry, Meselik Campus, Eskisehir, Turkey

ARTICLE INFO

Keywords:
Polymeric particles
Adsorption
Bromophenol blue
Phenol

ABSTRACT

Cellulose, activated carbon, zeolite, and similar materials have a weak effect against anionic pollutants. Therefore, further modifications are needed for the use of such substances. In this study, polymer particles (GD) that were economical and directly effective against anionic pollutants were synthesized as an alternative. GD particles were synthesized with glutaraldehyde and diethylenetriamine as monomers for the first time. The polymer particles were characterized in detail. Then, GD particles were used in the adsorption of anionic Bromophenol blue (BPB) and phenol (PH). As a result, it was determined that *i)* the adsorption process between GD particles, Bromophenol blue and phenol was chemisorption, *ii)* the adsorption of BPB and PH on to GD particles obeyed the Langmuir isotherm and pseudo second order kinetic model. pH, temperature, initial dye concentration, adsorbent dosage, and contact time were determined orderly 4, 50 °C, 300 mg L^{-1}, 10 mg, and 180 mins for BPB and 5, 50 °C, 10 mg L^{-1}, 15 mg, and 30 mins for PH. The maximum adsorption capacities of GD polymer particles for BPB and PH were ascertained as 136.40 mg g^{-1} and 98.26 mg g^{-1}, respectively. As a result, it was produced economical, simple, feasible, and functional adsorbents against anionic pollutants.

1. Introduction

Water pollution not only causes serious damage to the environment but also leads significant irreversible financial losses. Dyes and organic pollutants are two of the most important pollutant groups that cause water pollution [1–7]. Because every year, tons of dyes and organic pollutants from many industries such as food, paper, cosmetics, paint, textile, leather, pesticide and fertilizer are discharged uncontrollably into water resources [8,9]. To protect water resources, many methods have been developed for the treatment of dyes and organic pollutants [8,10–13]. However, it is accepted in the scientific world that adsorption is the most promising and successful method due to its advantages such as ease, energy efficiency, and cheapness [8,14–24].

Most of the dyes used in the industry are anionic dyes, and they contain disease-causing and carcinogenic groups [19,23,25–29]. In addition, they can change water resources' physical and chemical properties even at very low concentrations. BPB is widely used in the textile and printing industries and as an indicator in laboratory studies [30]. BPB was classified as acute toxic (dermal), serious eye irritant, and acute toxic (inhalation) by the European Chemicals Agency (ECHA) [31]. On the other hand, Phenols (PH) especially those containing chlorine, are considered priority pollutants [32]. PHs are environmentally important aromatic organic compounds and have attracted much attention recently due to their high toxicity to human and living health [33,34]. It is one of the primary pollutants in most chemical and petrochemical industries, such as coal refineries, paper, plastics, and agriculture.

Today, the common approach for effectively removing pollutants is using activated carbon (AC), zeolite, sepiolite, cellulose and similar natural materials as adsorbents because they are easily accessible and

* Corresponding author.
E-mail address: kgokkus@kastamonu.edu.tr (K. Gokkus).
[1] ORCID:0000–0002-4016–4283
[2] ORCID:0000–0002-8262–4882
[3] ORCID: 0000–0001-9942–6324
[4] ORCID:0000–0003-4542–5080

https://doi.org/10.1016/j.dwt.2024.100402
Received 27 February 2024; Received in revised form 7 May 2024; Accepted 16 May 2024

inexpensive. However, these adsorbents have very low effects against anionic pollutants due to the active groups on their surfaces. For example, it was determined that the natural composite material prepared with Fe_3O_4, CuO, and AC for the adsorption of BPB had an adsorption capacity of 88.60 mg g^{-1} [58]. In another study conducted with ACs produced from date pits, Eriochrome Balck T and BPB were removed [1]. As a result, it was observed that these ACs had an adsorption capacity of 36.5 and 39.68 mg g^{-1}, respectively. Another study used ACs produced from banyan root for PH adsorption [59]. Although the surface areas of these produced ACs were very high (988 m^2 g^{-1}), their PH removal capacity was relatively low (26.95 mg g^{-1}). Briefly, the inability to efficiently remove anionic pollutants with these natural adsorbents is an important problem. To overcome this problem, these materials must be modified. Adsorption capacities of these adsorbents against anionic pollutants can be increased only with modification. There are many studies in the literature for this purpose [28,58,60–63]. However, the modification process causes an additional problem to arise by increasing the cost of these natural adsorbents.

Glutaraldehyde (GA) is a highly reactive dialdehyde that reacts easily and quickly with nucleophiles such as amines, hydroxyls, and thiols under mild conditions. Therefore, GA used mostly as a cross-linking agent. Due to these advantages, it was used in scientific studies for many years [35–45]. Diethylenetriamine (DETA), on the other hand, contains three amine groups in its structure and therefore has high reactivity. Thus, it was used in materials science for many years in many different disciplines, from polymers to metals and biomaterials [46–57]. It is understood that both molecules will be used in many scientific studies in the future, as in the past, due to their high reactivity, cheap and high reaction efficiency. However, interestingly, in our literature research, we could not find the synthesis of polymer particles with GA and DETA. Therefore, in order to fill this major gap in the literature, GA and DETA were polymerized with high efficiency and ease in this study for the first time.

The main aim of this study was to synthesize new polymers that were effective directly against anionic pollutants, were low-cost, could be easily synthesized, and were alternatives to widely used adsorbents. This was achieved with polymer particles synthesized by polymerizing of GA and DETA for the first time. Within the scope of this study, two different models of anionic pollutants (Bromophenol blue, BPB, and phenol, PH) belonging to two different pollutant types (dyes and organic pollutants) were selected. GA and DETA used as monomers for the first time to obtain highly functional polymeric particles (GD). Adsorbents such as AC, zeolite or sepiolite have poor direct removal efficiency against anionic pollutants. When they are modified, they become uneconomical. As a solution to this problem, new adsorbent (GD) that was low-cost and directly effective on anionic pollutants was produced in this study. No further modification was required for these GD polymer particles.

2. Materials and Methods

2.1. Materials

Glutaraldehyde (25%, aqueous sol.) and DETA (99%) were purchased from Sigma Aldrich. EtOH (absolute), AC (99.5%), PH (99%) and THF (≥99.5%) were bought from Merck. BPB were purchased from AFG Scientific. All chemicals were used directly without extra purification.

2.2. Synthesis of GD polymer particles

After adding 80 mL (0.212 mol, 1.5 equivalents) of GA to the round bottom reaction flask, the balloon was closed with a septum to provide N_2 inert environment. Meanwhile, 15.25 mL (0.141 mol, 1.0 equivalent) of DETA was added to a separate vial, and the vial was closed with a septum similarly. Both solutions were degassed separately with N_2 gas for 20 min. Then, a cannula added the DETA solution to the GA solution at room temperature. The solution was stirred at a slow mixing speed until the formation of polymeric particles of tile color (the characteristic color of Schiff bases; Fig. 1). At the end of the reaction, GD particles were washed three times with distilled water (DW), ethanol (EtOH), acetone (Ac), tetrahydrofuran (THF), DW, and Ac, respectively. Thus, unreacted GA and DETA were removed. Finally, the particles were dried in a freeze dryer and made ready for characterization and adsorption.

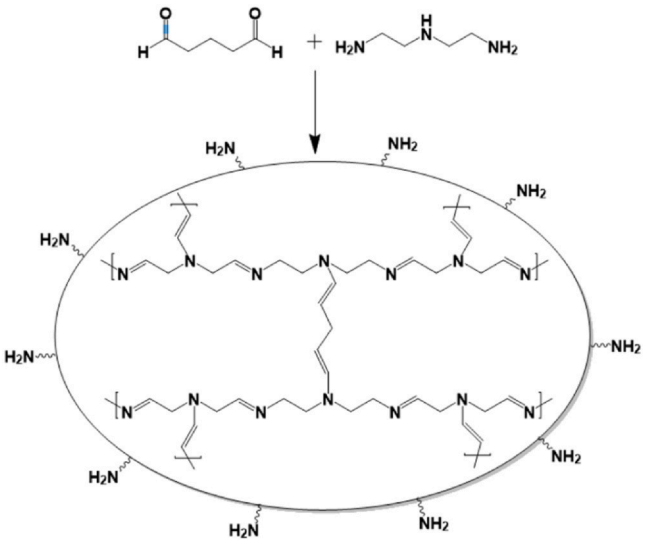

Fig. 1. Synthesis of GD polymer particles.

2.3. Characterization of GD polymer particles

SEM images for the morphologies of GD particles were obtained with the FEI Quanta FEG250 device. Chemical characterization was determined by Bruker Alpha model FT-IR instrument. Thermogravimetric analyses (TGA) were carried out with a Tetra SII Exster 6000 device at a rate of 5 °C/min in a nitrogen atmosphere between 25 °C and 800 °C.

2.4. Adsorption studies

All adsorption experiments were carried out in triplicate according to the batch adsorption method (Fig. 2). The effects of pH (2, 4, 6, 8, and 10), temperature (25, 35, 45 and 50 ºC), contact time (0 - 210 mins), initial dye concentration (40, 80, 100, 250, 300, 400, and 500 ppm) and GD dose (10, 25, 50, 75, and 100 mg) on the adsorption capacity of GD particles were completed according to the procedure reported by Shahbazi [64]. In all adsorption studies, the solution volume was 25 mL, and the shaking speed of 150 rpm was kept constant. The concentration or absorbance of BPB and PH solutions before and after the adsorption experiments were measured using the Hach Lange DR9000 UV Spectrophotometer at wavelengths 589 and 270 nm, respectively. The adsorption capacity and removal efficiency (%) of GD particles were calculated by Eqs. (I) and (II), respectively:

$$q_e = \frac{(C_o - C_e)}{W} \quad V \tag{I}$$

$$Removal\ Efficiency(\%) = \frac{(C_o - C_e)}{C_o} * \quad 100 \quad \% \tag{II}$$

where V (L) is the solution volume, Co and Ce (mg L^{-1} or ppm) represent the initial and final solution concentration of BPB dye, respectively, and W (g) is the adsorbed dry mass.

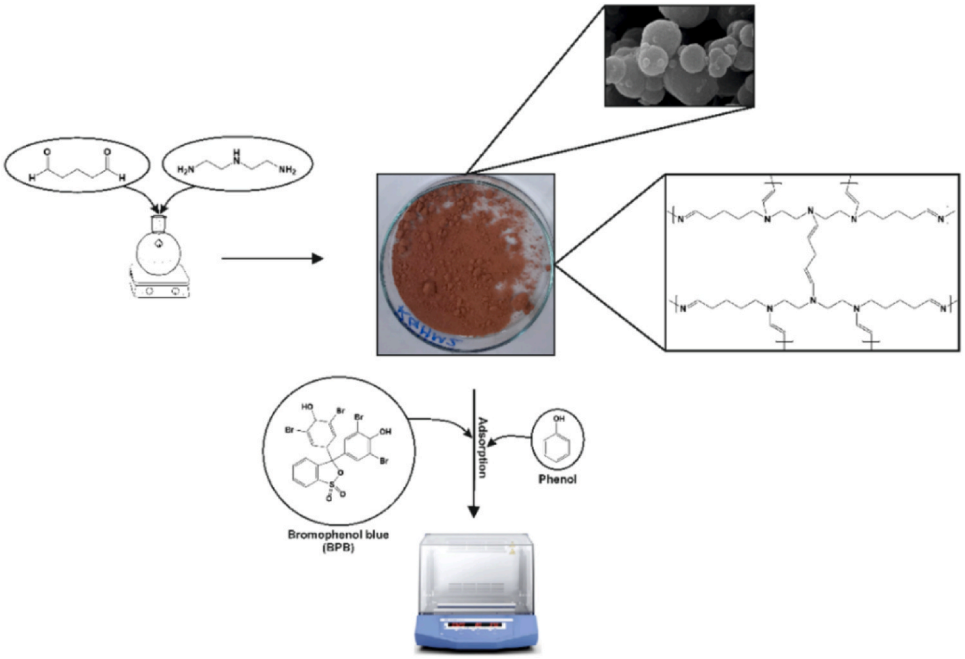

Fig. 2. Adsorption of BPB and PH with GD polymer particles.

3. Results and discussion

3.1. Synthesis approach

One of the goals of this study was the synthesis of polymers that were easily accessible, cheap, easy to synthesize and have high synthesis efficiency. Our main approach for this was to identify molecules that were highly reactive but economical. Our literature research showed that GA and DETA fit this approach. Because both molecules react rapidly under very mild conditions. In most of the studies, GA was used as a cross-linking agent and DETA was employed for modification purposes. They were not preferred as monomers until this study. In this study, GD polymer particles with GA and DETA were synthesized in very high yields (99.5%) under room conditions and in approximately one minute. These properties indicated that GD polymer particles had significant potential against conventional adsorbents.

3.2. Characterization

The chemical structure of the synthesized polymeric particles was revealed using FT-IR spectroscopy. The FT-IR spectra of all the samples were recorded in transmission mode using a Bruker-Alpha spectrometer ranging the wave number from 4000 to 400 cm^{-1}. The FT-IR spectrum of GD particles was shown in Fig. 3. Aliphatic -CH_2-stretching vibrations were observed in relatively broad bands under 3000 cm^{-1} at 2928 and 2862 cm^{-1}, while the peaks at 1439 and 1358 cm^{-1} were their bending vibrations. The broad peak at 3350 cm^{-1} was due to water adsorbed by GD particles, also seen in the TGA. Many peaks observed on this peak could belong to amine groups likely present in the resulting polymer end-groups. The strong peak in 1659 cm^{-1} was vibrations of imine groups (C=N), which were abundant in the structure of polymeric particles. On the left side of the imine peak, a peak (1697 cm^{-1}) belonging to the C=C binary group was seen as a shoulder. Additionally, an amine bending peak was observed at 1609 cm^{-1}.

The surface morphologies of GD particles were elucidated by SEM analysis. SEM micrographs obtained at different scales (200 and 500 nm and 2 μm) were given in Fig. 4. It was seen from the images that the polymer particles were successfully synthesized. Particle sizes were determined with the ImageJ software. The diameters of 106 different particles in the 2 μm SEM image were measured for this. Accordingly, it was determined that the average particle size was 703 nm, the smallest particle was 195 nm, and the largest particle was 1146 nm.

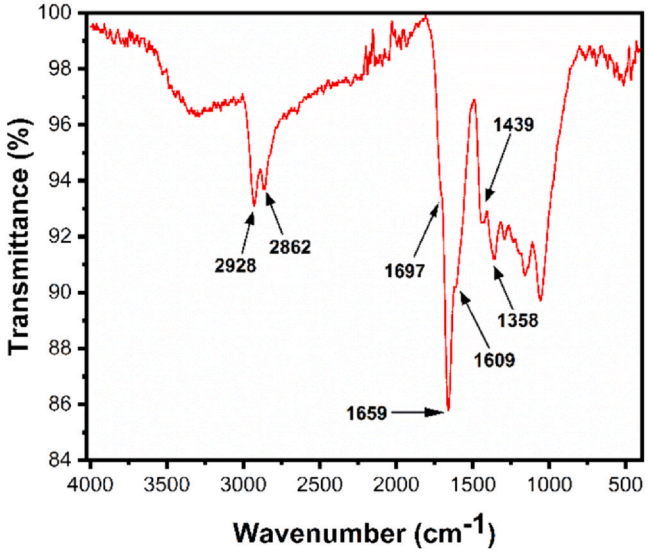

Fig. 3. FT-IR spectrum of GD polymer particles.

Thermal stability and decomposition of GD particles were determined by using TGA analysis. TGA analysis was conducted by heating the sample from room temperature to 800 ºC at a heating rate of 5 °C/min under a nitrogen atmosphere. The thermogram of GD particles was depicted in Figure S1. Accordingly, weight loss was seen in two stages. In the first stage, a weight loss of about 5% (5.26%) occurred in the weight of the polymer particles up to 105 ºC. The mass loss in this first stage was thought to be due to water loss. The second weight-loss stage started at 200 ºC and ended at 500 ºC. A weight loss of approximately 73% (73.11%) occurred at this stage. After the temperature of 200 ºC, the polymer particles started to decompose and completely decomposed at 500 ºC. After this second stage, approximately 22% (21.63%) of the mass remained as char.

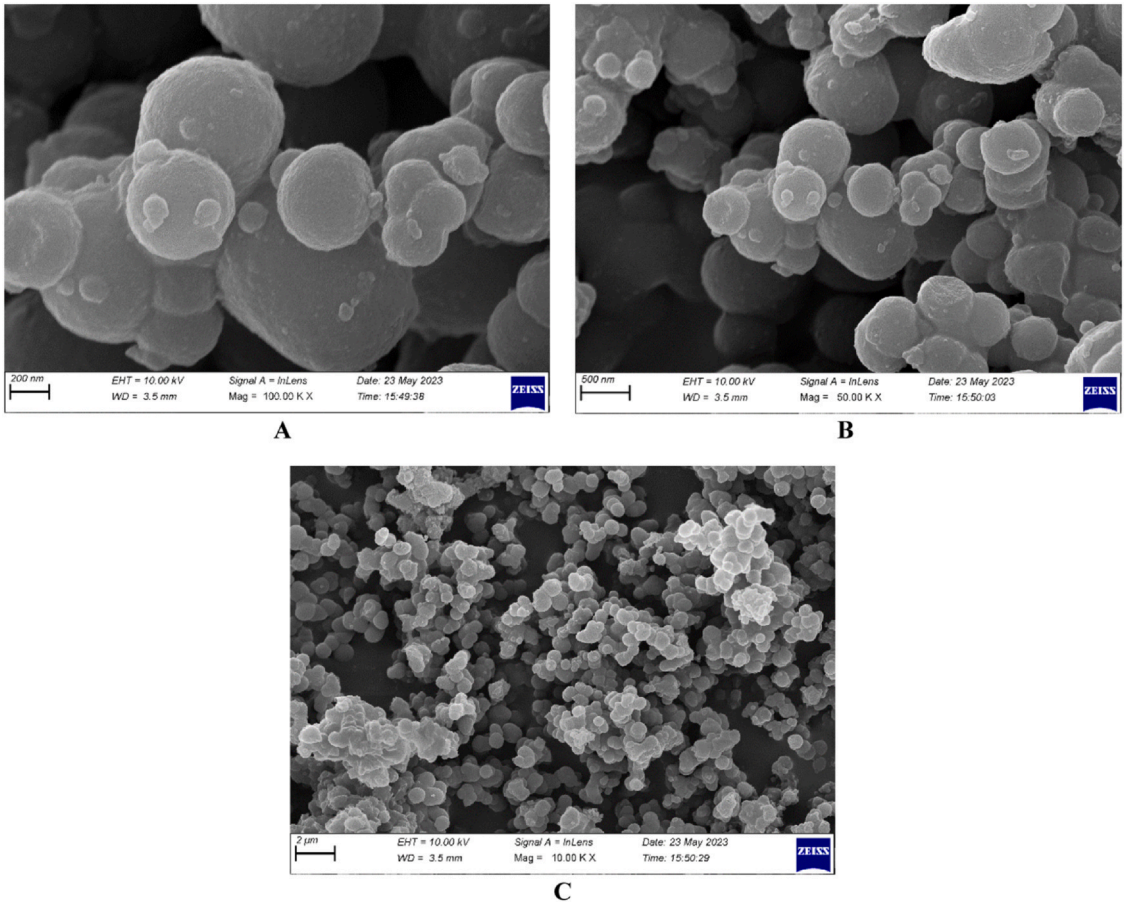

Fig. 4. SEM micrographs of GD polymer particles.

3.3. Adsorption experiments

3.3.1. Contact time effect and adsorption kinetics

Adsorption is an equilibrium process involving the interactions between adsorbate and adsorbent. Correctly determining the contact time between the adsorbate and the adsorbent is the first step for the most efficient use of the adsorbent. If this time is insufficient, the adsorption process cannot continue effectively. Otherwise, it will lead to a waste of time and energy. Therefore, this study determined contact times for BPB and PH first. Experiments were conducted between 0–210 min for BPB (300 mg L^{-1} BPB concentration, 25 ºC, and 50 mg GD particles) and 0–150 min for PH (pH 5.5, 25 ºC, 15 mg GD particles, 50 mg L^{-1} PH concentration) (Fig. 5). Accordingly, BPB was rapidly adsorbed on GD particles for up to 180 mins. After this time, this increase in adsorption stopped. Therefore, the adsorption contact time for BPB was determined to be 180 mins. A similar trend was observed for PH, and PH's contact time was 30 min. Subsequent experiments were carried out over these times. Due to physisorption between PH and GD particles, PH was adsorbed quickly on the surface of the polymer particles up to 30 mins. However, as adsorption progressed, the physical interactions between PH and GD particles weakened, and PH moved away from the surface (Fig. 5b). Conversely, chemisorption occurred between the BPB and GD particles. Since the chemical interaction is stronger than the physical interaction, the change in pH over time has not been observed in BPB (Fig. 5a).

Adsorption is a time-dependent process, and the equilibrium time is proportional to the adsorption rate. Therefore, the adsorption rate is essential when choosing an effective adsorbent to remove impurities from the solution [65]. Adsorption kinetics are calculated with this change in adsorption rate depending on time. These calculations determine the possible mechanism of dye adsorption on the adsorbent surface. Therefore, in order to understand the mechanism of adsorption between BPB, PH, and GD particles, the pseudo-first-order (PFO) kinetic model [66], pseudo-second-order (PSO) kinetic model [67], Weber-Morris intraparticle diffusion [68] and Elovich [69] kinetic models were used. Models and calculations were presented in the “Supplementary document.".

The results for the four models were given in Table 1, and the graphs obtained were given in Figures S2 and S3, respectively. The PFO model assumes that the occupancy rate of the adsorption sites is proportional to the number of occupied sites. In contrast, the PSO model considers that the occupancy rate of the adsorption sites is proportional to the square of the number of occupied sites [1,69]. Accordingly, when the correlation coefficients (R^2) calculated with the PFO and PSO models for BPB were compared, the R^2 of the PSO model was found to be higher (0.98). The adsorption for BPB fits the PSO kinetic model. This fitting showed that the rate-limiting step could be chemisorption involving valence forces through sharing or electron exchange between GD particles and BPB [19]. In addition, the adsorption energy in the Dubinin-Radushkevic (D-R) isotherm revealed that the adsorption had a chemical character. At the same time, when the calculated q_e (111.89 mg g^{-1}) and experimental q_e (94.33 and 99.8 mg g^{-1}, respectively) amounts for both models were compared, it was understood that the PSO model was more appropriate for the adsorption.

Adsorption generally occurs in three mass transfer stages, depending on time. The first is the external diffusion of dye molecules in the liquid phase to the adsorbent surface. The second is the intraparticle diffusion of dye molecules into the pores of the adsorbent, and the third is the formation of physical or chemical bonds of the adsorbate at the active centers in the pores of the adsorbent [3]. Therefore, the linearity of the graphs obtained by kinetic studies does not cover the entire time interval. They exhibit multicollinearity, revealing the existence of

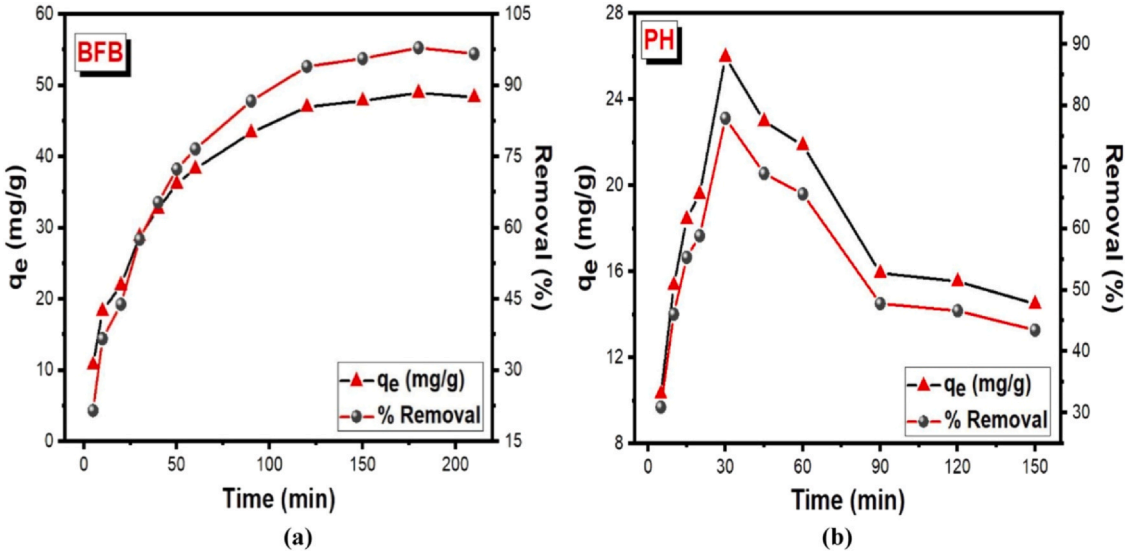

Fig. 5. Effects of contact time on (a) BPB adsorption (initial conc.: 100 mg L^{-1}; T: 25 ºC; adsorbent: 50 mg; V: 25 mL) and (b) PH adsorption (pH:5.5; initial conc. 50 mg L^{-1}; adsorbent 15 mg, V:10 mL, T:25 °C, 400 rpm).

Table 1
Kinetic parameters of PH and BPB adsorption on GD particles.

Models	Parameters	GD particles	
		PH	BPB
Pseudo-first order	q_e (mg.g^{-1})	23.8	111.89
	k_1 (min^{-1})	0.08	-0.016
	R^2	0.9936	0.970
	q_{exp} (mg.g^{-1})	25.98	94.33
Pseudo-second order	q_e (mg.g^{-1})	25.32	111.89
	k_2 (g.mg^{-1}.min^{-1})	0.01	0.00036
	R^2	0.9968	0.98
	q_{exp} (mg.g^{-1})	25.98	99.8
Weber-Morris	k_i (mg. $g^{-1}min^{-1/2}$)	4.24	3.05
intra-particle	I (mg.g^{-1})	1.34	10.49
diffusion	R^2	0.9694	0.90
Elovich	α (mg.$g^{-1}min^{-1}$)	6.33	5,28
	β (g.mg^{-1})	0.145	0088
	R^2	0.9929	0,98

successive adsorption steps. The adsorption process between GD particles and BPB occurred in two stages, as seen in the graph obtained by Weber-Morris intraparticle diffusion (Figure S3c). Accordingly, the adsorption capacity increased rapidly up to 43.36 mg g^{-1} in the first stage, and then this increase rate slowed down in the second stage. Since the active sites on the surface of GD particles were empty at the beginning of the adsorption (first step), BPB molecules were rapidly adsorbed to these sites. Therefore, in the first stage, adsorption took place rapidly. In the second step, where the adsorption rate decreased, BPB molecules diffused into the macro pores of GD particles. Therefore, the rate of adsorption decreased. When the Weber-Morris diffusion diagram within the particles was examined to determine the rate-limiting step of the adsorption mechanism (Figure S3c), it was found that PH adsorption occurs in two stages. In the first stage, intraparticle diffusion was active, where PH ions moved towards the surface where adsorption took place into the pores of the GD particles. In the second phase, the adsorption equilibrium part was observed, where the intraparticle diffusion slowed down as less PH concentration remained in the solution and the pores of the GD particles were more filled.

The Elovich equation is a kinetic model that explains chemical adsorption on heterogeneous solid surfaces. The correlation coefficient (R^2 = 0.98) showed that the fit of this model was the same as for PSO. These results showed that the adsorption between GD particles and BPB fits the PSO and Elovich kinetic model. In other words, it was understood that the surface of GD particles was heterogeneous, and chemical adsorption took place between GD particles and BPB. When the kinetic models for PH adsorption were examined, the correlation coefficient (0.9968) was higher in the PSO kinetic model. At the same time, the calculated $q_{e,cal}$ values (25.32 mg g^{-1}) were extremely close to the experimental $q_{e,exp}$ value (25.98 mg g^{-1}). Thus, the PSO kinetic model proved to be more suitable to represent the kinetics of PH adsorption on GD particles (Table 1). As is well known, the PSO model is based on the hypothesis that valence forces can control the rate-limiting step through electron sharing or exchange between adsorbent and adsorbate [37]. This result was also consistent with the kinetic behavior of PH adsorption on other adsorbents [70,71]. In summary, the PSO kinetic model, which fitted well with PH adsorption, showed that the adsorption process was due to the interaction between the π-electrons in the PH ring and the basal plane of GD particles [72].

3.3.2. *Effect of pH*

pH changes the surface charge of the dyes and adsorbents and the degree of protonation of the functional groups in the adsorbent. In short, since the change in pH seriously affects the adsorption process, it is necessary to determine the optimum pH. Therefore, experiments were conducted with GD particles for the adsorption of BPB dye at different pHs (2, 4, 6, 8, and 10) (25 ºC, 50 mg GD particles, 100 ppm BPB concentration, and 180 min). Accordingly, the lowest BPB adsorption was determined at pH 10 (32.44 mg g^{-1}) and the highest at pH 4 (48.85 mg g^{-1}) (Fig. 6a). The adsorption efficiency decreased as pH increased. BPB is a weakly acidic dye. Therefore, BPB is anionic below pH 7 [2,4,73,74]. Briefly, BPB is anionic at pH 2, 4 and 6 and ionic at pH 8 and 10. On the other hand, Zeta Potential measurements (25.5 mV and 0.0802 ms cm^{-1}) at pH 7 showed that the surface of GD particles was cationic (Figure S4). In addition, GD particles had amino groups in their structure. It was also well known that amino groups become quaternized by protonation in acidic medium and acquire cationic properties. In an acidic environment, the cationic character of GD polymer particles increased. Thus, the electrostatic interactions between BPB molecules and GD polymer particles became stronger in acidic conditions. As a result, the highest adsorption efficiency was achieved at pH 4. After pH 8, the interaction between BPB dye and GD particles weakened due to deprotonation of amine groups. As a result of this, the adsorption efficiency decreased significantly at pH 10. In addition, Ghaedi [2] also obtained similar results. Furthermore, it was

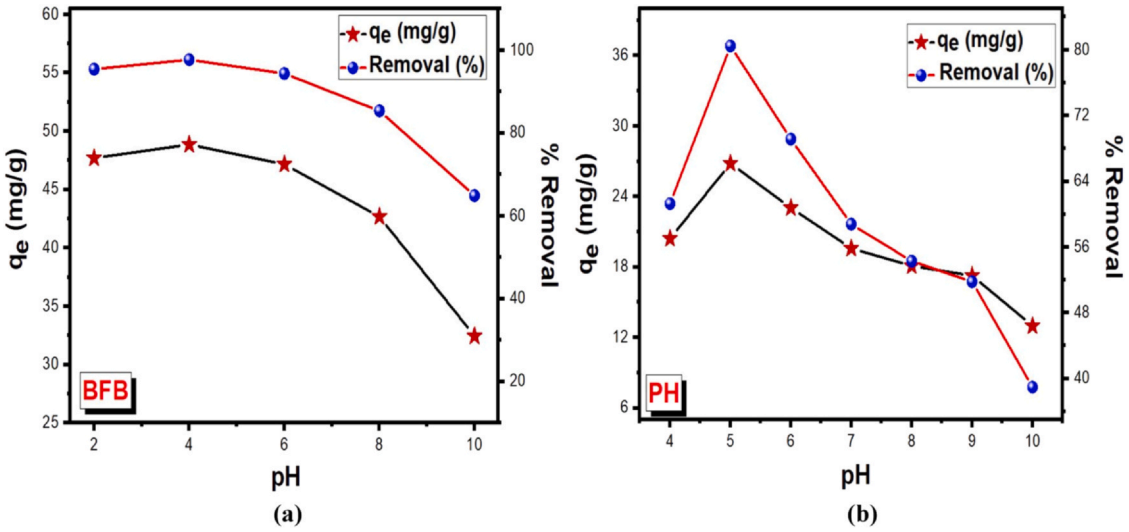

Fig. 6. Effects of pH on (a) BPB (t: 180 min; concentration: 100 mg L^{-1}; T: 25 ºC; adsorbent: 50 mg; V: 25 mL) and (b) phenol adsorption (t: 30 min; initial conc. 50 mg L^{-1}; adsorbent 15 mg, V:10 mL, T:25 ˚C, 400 rpm).

known that the adsorption of anionic dyes decreased with increasing pH, and the adsorption of cationic dyes increased [75]. On the other hand, to determine the optimum pH for PH adsorption onto GD particles, experiments were performed between pH 4 and 10 (30 min, 25 ºC, 15 mg GD, 50 mg L^{-1} PH concentration). The amount of adsorbed PH reached its maximum value at pH 5 and tended to decrease at higher and lower pH values (Fig. 6b). This decrease in pH values other than pH 5 may be due to the anionic character of PH and the cationic character of GD particles, as in BPB adsorption. Adsorption of PH molecules was adversely affected due to the suppression of increased proton and hydroxyl groups in the environment [76]. While PH becomes protonated and has a cationic charge up to pH 5, PH acquires a neutral character above 5 and an anionic character at higher pHs. Therefore, PH adsorption was highest at pH 5. In a more acidic environment, protons competed with PH and adsorbed faster to the surface of GD particles. As a result, PH removal decreased at lower pH.

3.3.3. *Initial BPB and PH concentration effects and adsorption isotherms*

Determining the optimum dye concentration for an adsorbent is one of the essential parameters to reveal the use potential or capacity. Therefore, with different initial BPB concentrations (40 – 500 mg L^{-1}), the optimal BPB concentration for GD particles was determined (25 ºC, 50 mg GD particles, and 180 min; Fig. 7a). The adsorption efficiency of GD particles increased rapidly from 40 mg L^{-1} to 300 mg L^{-1} concentration (from 19.23 mg g^{-1} to 111.90 mg g^{-1}), after which the increase did not change much (from 111.90 mg g^{-1} to 116.58 mg g^{-1}). Up to 300 mg L^{-1} concentration, BPB molecules were rapidly adsorbed on the surface of GD particles, after which the adsorption rate decreased markedly. This rapid increase could be explained by the increasing amount of BPB molecules repel each other. Under the influence of this possible repulsion, BPB molecules rapidly diffused to the surface of GD particles. This may have triggered both faster adsorption and better diffusion of particles into the pores of GD particles. As a result, 300 mg L^{-1} was determined as the most suitable BPB concentration for GD adsorbent.

Regarding PH, the effect of different initial concentrations (5–250 mg L^{-1}) was demonstrated by shaking the PH solution at 15 mg GD particles and pH 5 for 30 min (Fig. 7b). Accordingly, the highest PH removal efficiency was 88.9% for the initial 10 mg L^{-1} PH concentration. Adsorption sites and specific adsorbent surfaces were more

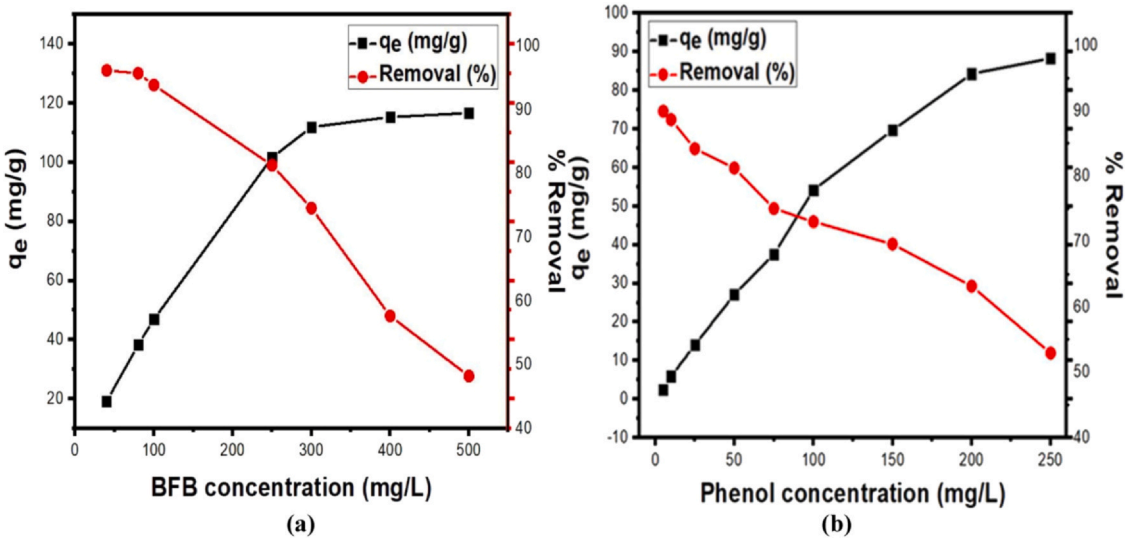

Fig. 7. Effects of initial concentration on (a) BPB (t: 180 min; pH: 4.0; T: 25 ºC; adsorbent: 50 mg; V: 25 mL) and (b) phenol adsorption (t: 30 min; pH: 5.0; adsorbent 15 mg, V:10 mL, 400 rpm).

Table 2
Isotherm parameters of phenol and BPB adsorption on GD particles.

Models	Parameters	GD particles	
		PH	BPB
Langmuir	q_{max} ($mg.g^{-1}$)	107.53	120.48
	$q_{e,exp}$ ($mg.g^{-1}$)	98.26	111,89
	K_L ($L.mg^{-1}$)	0.04	0.13
	R_L	0.7	0.16
	R^2	0.9941	0.9998
Freundlich	K_f [$(mg.g^{-1})(L.mg^{-1})^{1/n}$)]	6.27	22.45
	n	1.66	2.97
	R^2	0.9811	0.903
Temkin	β_T	19.5	20.43
	KT ($L.g^{-1}$)	0.72	1.93
	R^2	0.9536	0.963
Dubinin-Radushkevich	q_{max} ($mg{\cdot}g^{-1}$)	50.82	89.35
	$q_{e,exp}$ ($mg.g^{-1}$)	98.26	111,89
	β ($mol^{-2}.\ J^{-2}$)	$0.9 * 10^{-5}$	$1.04 * 10^{-6}$
	E ($kJ.mol^{-1}$)	235.7	692.26
	R^2	0.6817	0.979

attractive at low PH concentrations, so the removal efficiency was high. In the opposite case, the removal efficiency decreased due to the saturation of the adsorption areas quickly [76].

Experimental data tests in Langmuir [77], Freundlich [78], Tempkin [79], and Dubinin-Radushkevich [80] isotherm models were performed for this study to evaluate the adsorption equilibrium process and to comprehensively investigate and reveal the interaction between BPB, PH and GD particles. Details of models and calculations were given in the "Supplementary document.".

Parameters of all isotherms for BPB and PH adsorption on GD particles were presented in Table 2, and graphs of isotherms were depicted in Figures S5 and S6, respectively. Isotherm calculations and graphs for BPB were created using data obtained with 300 ppm BPB concentration. Accordingly, the highest R^2 value of 0.9998 among all isotherms for BPB was obtained in the Langmuir isotherm. This showed that the adsorption was monolayer and homogeneous. The calculated q_m and experimental q_e results (120.48 mg g^{-1} and 111.89 mg g^{-1}, respectively) also supported these results. On the other hand, the adsorption energy (119.02 J mg^{-1}) calculated for BPB with the Temkin isotherm clearly revealed that the adsorption process was endothermic. Therefore, there was a strong interaction between BPB and GD particles. It was also explained in the section where the effect of temperature on adsorption was explained that the adsorption process was endothermic (Fig. 9). In order to decide on the adsorption type, the adsorption energy values calculated from the D-R adsorption isotherm were used. The fact that the adsorption energy calculated by the D-R isotherm (E = 691.07 kJ mol^{-1}) was greater than 16 kJ mol^{-1} indicated a chemical adsorption process between GD particles and BPB.

As in BPB, the highest R^2 (0.9941) was determined for PH adsorption in the Langmuir model. This showed that PH molecules were adsorbed on the GD particles' surface in a monolayer and homogeneous manner. The fact that the maximum monolayer adsorption capacity (q_m; 107.53 mg g^{-1}) calculated from the Langmuir isotherm model was very close to the experimental results (q_e; 98.26 mg g^{-1}) supported that monolayer adsorption took place. Similarly, Sridar [81] in their study of PH adsorption on zinc oxide (ZnO) nanoparticles, stated that Langmuir isotherm showed good agreement with PH removal data compared to other isotherms. Another study, which determined the PH adsorption capacity with clay-carbon composites, reported that the Langmuir isotherm was the most suitable isotherm model for adsorption [82]. The n values calculated from the Freundlich isotherm equation were 1.66 for PH. Since this value was in the range of $1 < n < 10$, it can be concluded that adsorption was feasible. The adsorption energy calculated with the D-R isotherm (E = 235.7 kJ mol^{-1}) for PH adsorption is greater than 16 kJ mol^{-1}, indicating that a chemical adsorption process takes place between GD particles and PH.

3.3.4. Adsorbent dosage

Determining the optimum amount of adsorbent for adsorption is very important in terms of not decreasing the adsorption efficiency and increasing the cost. If the amount of adsorbent is kept low, the surface area of the adsorbent and the number of active sites will not be sufficient to adsorb the dye at the desired concentrations. The use of high amount of adsorbent will not be economical. Therefore, experiments were conducted to determine the optimum amount of adsorbent (between 10 and 100 mg) (25 ºC, 100 ppm BPB concentration, and 180 min). Accordingly, the adsorption efficiency of GD particles decreased as the amount of adsorbent increased. The highest adsorption capacity was determined at the amount of 10 mg adsorbent (104.10 mg g^{-1}), and the lowest capacity was determined at the amount of 100 mg adsorbent (22.98 mg g^{-1}) (Fig. 8a). The agglomeration of GD particles could explain the decrease in adsorption efficiency with the amount of adsorbent during the process (it may be that the agitation speed was insufficient for the amount of adsorbent 100 mg). The possibility of agglomeration of GD particles made it difficult for BPB molecules to diffuse into or onto the adsorbent surface. Therefore, this effect was dominant above the amount of 100 mg adsorbent. Similar results were obtained in highly cross-linked polyamine folic acid (PFCs) polymers synthesized by the polycondensation technique [19]. In the adsorption of Congo red, it was stated that the active sites were closed due to agglomeration of the polymers, and the adsorption efficiency decreased. In experiments to determine the effect of adsorbent dose on PH adsorption, despite the amount of adsorbent varying in the range of 5–120 mg, the initial PH concentration was 50 mg L^{-1}, contact time 30 min, pH 5, temperature adjusted to 25 °C (Fig. 8b). Maximum adsorption efficiency (85.2%) was obtained when the adsorbent dose was 15 mg. As the amount of adsorbent increased, the adsorption efficiency decreased.

3.3.5. Effect of temperature and chemical thermodynamics

Experiments were carried out at different temperatures (15 – 50 ºC) (50 mg GD particles, 100 ppm BPB concentration, and 180 min) to investigate the effect of temperature on the adsorption process. Accordingly, the lowest result (112.231 mg g^{-1}) was obtained at 25 ºC and the highest (136.40 mg g^{-1}) at 50 ºC. Results increased slightly from 25 ºC to 45 ºC (Fig. 9a). At 50 ºC, the adsorption efficiency reached its maximum level with a sudden increase. This continuous increase indicated that the adsorption process was endothermic. In

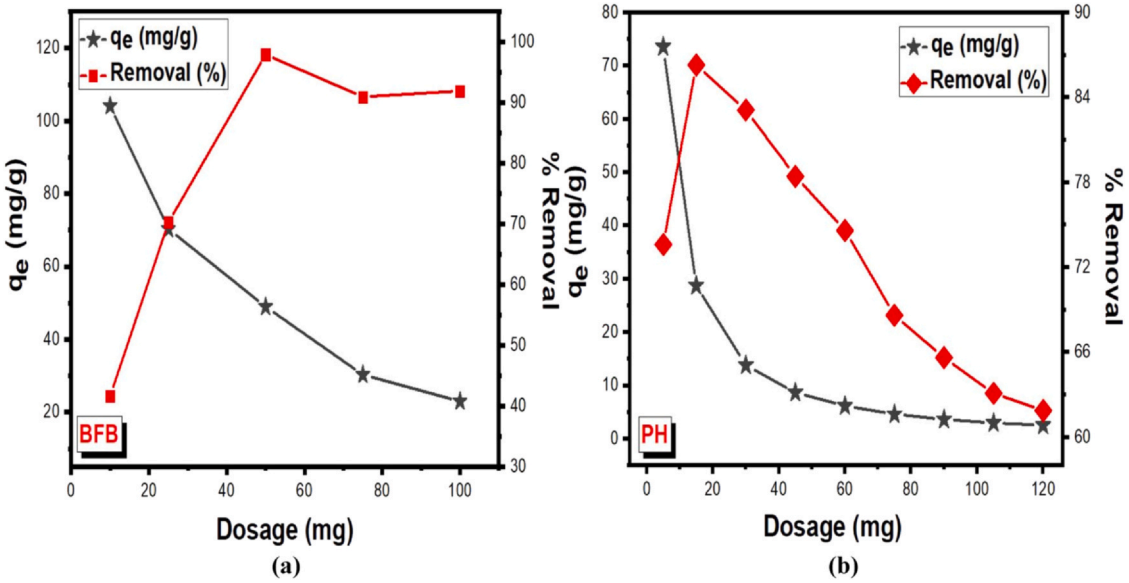

Fig. 8. Effects of adsorbent dosage on (a) BPB (t: 180 min; concentration: 100 mg L^{-1}; pH: 4.0; T: 25 ºC; adsorbent: 50 mg; V: 25 mL) and (b) phenol adsorption (t: 30 min; pH: 5.0; adsorbent 15 mg, V:10 mL, 400 rpm).

other words, as the temperature increased, more BPB molecules were adsorbed on the surface of GD particles. In order to determine the effects of temperature on PH adsorption, at temperatures ranging from 20–50 ºC, PH solutions at an initial concentration of 50 mg L^{-1} at pH 5.0 were shaken for 30 min. As the temperature increased, the adsorption capacity increased, as shown in Fig. 9b. The optimum temperature value was found to be 50 ºC. This showed that the adsorption reaction also occurred endothermically for PH. For both BPB and PH, the adsorption efficiencies of GD particles increased with the increase in temperature. The kinetic energy increased with increasing temperature. This increase in kinetic energy made it easier to overcome the mass transfer resistances between BPB and PH molecules and GD particles [30]. In this case, it explained the increase in efficiency of BPB and PH adsorption as the temperature increases. Similar results obtained in the literature [18,30,72].

Evaluation of the adsorption process from a thermodynamic point of view is critical to deciding whether adsorption is spontaneous. In this study, these evaluations were made using thermodynamic parameters such as Gibbs free energy, enthalpy, and entropy changes. The equations used for the calculations were given in the "Supplementary document.".

In order to calculate the adsorption thermodynamic function values such as ΔG°, ΔS° and ΔH°, adsorption experiments were carried out at 25, 35, 45 and 50 °C with 300 ppm BPB concentration and 50 mg GD particles. The adsorption process usually takes place at constant pressure. Therefore, the thermodynamic function Gibbs free energy change (ΔG°) was used to decide whether the adsorption process was stable at constant pressure. Since the reaction changes with time or the adsorption process takes place, whether the reaction is spontaneous is determined by the decrease or increase of ΔG° [83]. When the data in Table 3 were examined, it was determined that the ΔG° value calculated for all temperatures varied between − 0.98 and − 4.33 kJ mol^{-1}. The negative Gibbs free energy indicated that adsorption was voluntary and spontaneous for BPB. The standard enthalpy change (ΔH°) represented the heat change for reactions under constant pressure. A negative value indicated that the system gave off heat (exothermic), and a positive value indicated that the reaction received heat (endothermic). As a result of the calculations, the ΔH° value was found to be 31.96 kJ

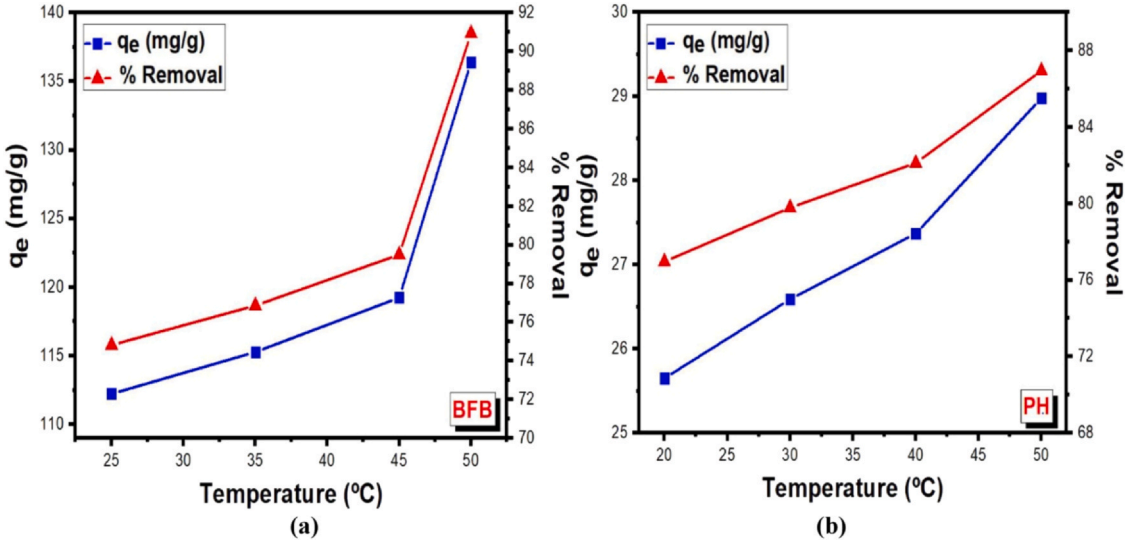

Fig. 9. Effects of temperature on (a) BPB (t: 180 min; concentration: 100 mg L^{-1}; pH: 4.0; adsorbent: 50 mg; V: 25 mL) and (b) phenol adsorption (t: 30 min; pH: 5.0; initial conc. 50 mg L^{-1}; adsorbent 15 mg, V:10 mL, 400 rpm).

Table 3
Thermodynamics parameters of phenol and BPB adsorption on GD particles.

	Temp. (K)	ΔH° (kJ mol^{-1})	ΔS° (J mol^{-1}K^{-1})	TΔS° (kJ mol^{-1})	ΔG° (kJ mol^{-1})
Phenol	293	17.96	70.79	20.74	-2.95
	303			21.45	-3.45
	313			22.16	-3.96
	323			22.87	-5.05
BPB	298	31.96	109.22	32.55	-0.98
	308			33.64	-1.30
	318			34.73	-1.75
	323			35.28	-4.33

Table 4
Optimum adsorption conditions for BPB and PH with GD particles (Optimum adsorption conditions regarding BPB and PH interaction with GD particles).

	BPB	PH
pH	4	5
Temperature (°C)	50	50
Initial concentration (mg L^{-1})	300	10
GD dosage (mg)	10	15
Contact time (min)	180	30

mol^{-1}. That was, the adsorption between GD particles and BPB was endothermic. This showed why the adsorption efficiency between GD particles and BPB increased with increasing temperature. If the standard entropy change (ΔS°), which indicates the disorder in the reaction, is positive, the randomness increases during adsorption. As a result of the experiments, the ΔS° value of 109.22 J mol^{-1} K for GD particles indicated that the adsorption at the GD particles and BPB interface increased irregularity.

Thermodynamic parameters calculated for PH adsorption on GD particles were also given in Table 3. Accordingly, negative ΔG° values (−2.95 and −5.05 kJ mol^{-1}), as in BPB, indicated that PH adsorption was a spontaneous and positive process. In addition, the fact that the ΔG° value becomes more negative with increasing temperature confirmed that increasing temperature supported adsorption. On the other hand, it was observed that the entropy changes also contributed to the negative ΔG° value. Regarding standard enthalpy change, the magnitude of ΔH° showed that the adsorption was chemisorption [84]. Therefore, it was understood that PH adsorption on GD particles took the form of chemisorption. A positive ΔS° value increased the randomness of the solid-solution interface during the adsorption reaction [85]. The increase in temperature promoted stabilization of the bonds between the binding sites on the PH molecules and GD particles, indicating that the high temperature promoted the adsorption process. Like thermodynamic behaviors, Lütke [61] also found PH adsorption on activated carbon from black acacia bark.

Optimum conditions for BPB and PH were determined in the experiments carried out with different pH, temperature, initial pollutant concentration, and adsorbent dosage (Table 4).

In the literature, studies on the adsorption of BPB dye, especially with polymers, are very few compared to other dyes [30]. For PH, there are more studies conducted. In Table 5, the results obtained in the literature for both BPB and PH adsorption were summarized. In terms of BPB, it was understood that polymers had lower adsorption capacity compared to other dyes. The highest adsorption capacity (136.40 mg g^{-1}) was achieved with GD polymer particles, while the lowest capacity (7.43 mg g^{-1}) was with azo-dye-functionalized superparamagnetic iron oxide nanoparticles polymers. When the results were examined, it was seen that GD polymer particles were on average 7.88 times more effective against BPB dye than in the literature. We thought that two strong interactions led to these results. The first was the strong hydrogen bonds formed between the hydrogens of amine groups in the structure of GD particles and the hydroxyl, sulfonate groups, and aromatic structures in the BPB dye. The second was the π-π interactions that could occur between pi bonds of imine groups and aromatic rings. The situation was different in terms of PH. It was seen in the literature that higher results were achieved. The highest PH adsorption (318.6 mg g^{-1}) was obtained with acylamino-functionalized hyper-cross-linked polymers and the lowest (16.52 mg g^{-1}) with Fe_3O_4 @SiO_2 magnetic double-network nanocomposite. It was concluded that the interactions between the amine and imine groups in the structure of GD polymer particles and the -OH and phenyl groups of PH were weaker. Therefore, the capacity of GD polymer particles against PH was relatively low (98.26 mg g^{-1}) compared to the literature. Moreover, the high PH adsorption capacities in the literature were obtained with hyper cross-linked polymers. Hyper cross-linked polymers are rich in

Table 5
Comparison of the results obtained for BPB and PH with other studies in the literature.

Pollutants	Adsorbent	Capacity (q_e, mg g^{-1})	Kinetics	Isotherm	References
BPB	GD particles	136.40	PSO	Langmuir	This work
	PAN nanofibers	42.017	PSO	Freundlich	[88]
	PAN-CD nanofibers crosslinked with citric acid	79.365	PSO	Freundlich	
	Polymer-clay composite	10.7	PFO	Freundlich	[89]
	Polyethyleneimine-coated SPIONs	11.3	PSO	Freundlich	[87]
	Azo-dye-functionalized superparamagnetic iron oxide nanoparticles	7.43	PSO	Freundlich	[90]
	PAN@SiO_2 nanocomposites	129.6	PSO	Langmuir	[91]
	CNP	22.72	PSO	Langmuir	[18]
PH	GD particles	98.26	PSO	Langmuir	This work
	PCNS-gel	104.2	PFO	D-R	[92]
	Acylamino-functionalized hyper-cross-linked polymers	318.6	PSO	Langmuir	[93]
	Hydroxyl-functionalized hypercrosslinked polymers	156.74	PSO	Freundlich	[94]
	PS-PDAT-FDA($SnCl_4$)	214.5	PFO	Freundlich	[95]
	Acrylate-functionalized hyper-cross-linked polymers	163.6	-	Langmuir	[96]
	Collagen-(AMPS-MAA/AAm)-Fe_3O_4 @SiO_2 magnetic double-network nanocomposite	16.52	PSO	Langmuir	[97]

hetero atoms and aromatic groups. They also have high surface area and pore volumes. These properties of hyper-cross-linked polymers led significantly to increase PH adsorption. On the other hand, phenol in wastewater has been found at various concentrations ranging from $< 10\ mg\ L^{-1}$ to several thousands of $mg\ L^{-1}$ [86]. For example, wastewater from the resin industry (600–2000 $mg\ L^{-1}$), refineries (6–500 $mg\ L^{-1}$), petrochemical (2.8–1220 $mg\ L^{-1}$), coal (28–3900 $mg\ L^{-1}$) and pulp, and paper, pharmaceutical, plastic and paint processing industries (0.1–1600 $mg\ L^{-1}$) contain very high PH concentrations [87]. According to these concentrations, it iss understood that the adsorbents produced in the literature and in this study may be insufficient for PH adsorption, or very high amounts of adsorbents will need to be used for adequate PH removal. Using high amounts of adsorbent will not be economical. Therefore, much more adsorbents should be used for efficient PH removal.

4. Conclusion

Dye and organic materials are two of the most severe pollutants for water resources due to i) their high production and use and ii) their high potential as pollutants. Both types of pollutants cause rapid changes in water resources' physical and chemical properties. This change adversely affects the health and life of all living things. Therefore, high-efficiency anionic BPB and PH adsorption were aimed to protect water resources in this study.

Within the scope of the study, anionic pollutants were selected. Because adsorption of anionic pollutants remains a severe problem in synthetic supramolecular chemistry. Thus, an essential approach to this problem was presented in this study. Polymeric particles were synthesized quickly with Schiff base chemistry using GA and DETA as monomers for the first time. Appropriate characterization methods proved the successful synthesis of GD particles.

The batch adsorption method was used for BPB and PH. As a result, it was determined that GD polymer particles had a very high capacity of 136.40 $mg\ g^{-1}$ for BPB and 98.26 $mg\ g^{-1}$ for PH. In addition, the mechanism of adsorption was elucidated by adsorption isotherms (Langmuir, Freundlich, Temkin, and D-R), adsorption kinetics (PFO, PSO, W-M intra-particle diffusion, and Elovich), and thermodynamic parameters (Gibb's free energy, enthalpy, and entropy). Thus, it was understood that the adsorption process between GD particles, Bromophenol blue and phenol was chemisorption. It was also determined that the adsorption of BPB and PH on to GD particles obeyed the Langmuir isotherm and PSO kinetic model. The pH, temperature, initial dye concentration, GD dosage, and contact time were ascertained orderly 4, 50 °C, 300 $mg\ L^{-1}$, 10 mg, and 180 mins for BPB and 5, 50 °C, 10 $mg\ L^{-1}$, 15 mg, and 30 mins for PH.

In this study, very fast and easy to synthesize, and cheap polymeric particles were synthesized. It was demonstrated that these polymers could be used successfully against BPB and PH, which were important regarding water pollution. The polymeric particles obtained with this synthesis approach are believed to shed important light on future studies.

CRediT authorship contribution statement

Kutalmis Gokkus: Writing – review & editing, Writing – original draft, Methodology, Investigation, Conceptualization. **Cigdem Oter:** Writing – original draft, Methodology, Investigation, Conceptualization. **Merilyn Amlani:** Methodology, Investigation, Formal analysis. **Mahmut Gur:** Writing – review & editing, Writing – original draft, Investigation, Conceptualization. **Vural Butun:** Writing – review & editing, Supervision, Funding acquisition.

Declaration of Competing Interest

The authors declare that they have no known competing financial interests or personal relationships that could have appeared to influence the work reported in this paper.

Data availability

The authors do not have permission to share data.

Appendix A. Supporting information

Supplementary data associated with this article can be found in the online version at doi:10.1016/j.dwt.2024.100402.

References

[1] Altaher H, Khalil TE, Abubeah R. The effect of dye chemical structure on adsorption on activated carbon: a comparative study. Color Technol 2014;130(3):205–14.
[2] Ghaedi M, et al. Random forest model for removal of bromophenol blue using activated carbon obtained from Astragalus bisulcatus tree. J Ind Eng Chem 2014;20(4):1793–803.
[3] Ahmed M, Abou-Gamra Z. Mesoporous MgO nanoparticles as a potential sorbent for removal of fast orange and bromophenol blue dyes. Nanotechnol Environ Eng 2016;1(1):11.
[4] Xiang Y, et al. Comparative study of three novel organo-clays modified with imidazolium-based gemini surfactant on adsorption for bromophenol blue. J Mol Liq 2019;286:110928.
[5] Khan NA, et al. Efficient photodegradation of orange II dye by nickel oxide nanoparticles and nanoclay supported nickel oxide nanocomposite. Appl Water Sci 2022;12(6). https://doi.org/10.1007/s13201-022-01647-x.
[6] Zahoor M, et al. Novel Magnetite Nanocomposites (Fe_3O/C) for Efficient Immobilization of Ciprofloxacin from Aqueous Solutions through Adsorption Pretreatment and Membrane Processes. Water 2022;14(5). https://doi.org/10.3390/w14050724.
[7] Lakkaboyana SK, et al. Synthesis and characterization of $Cu(OH)_2$-NWs-PVA-AC Nano-composite and its use as an efficient adsorbent for removal of methylene blue. Sci Rep 2021;11(1). https://doi.org/10.1038/s41598-021-84797-3.
[8] Umar A, et al. Synthesis and characterization of Pd-Ni bimetallic nanoparticles as efficient adsorbent for the removal of acid orange 8 present in wastewater. Water 2021;13(8):1095.
[9] Lakkaboyana SK, et al. Synthesis of copper oxide nanowires-activated carbon (AC@CuO-NWs) and applied for removal methylene blue from aqueous solution: Kinetics, isotherms, and thermodynamics. J Inorg Organomet Polym Mater 2019;29:1658–68.
[10] Alam S, et al. Preparation of activated carbon from the wood of Paulownia tomentosa as an efficient adsorbent for the removal of acid red 4 and methylene blue present in wastewater. Water 2021;13(11):1453.
[11] Alam S, et al. Preparation of Pd–Ni nanoparticles supported on activated carbon for efficient removal of basic blue 3 from water. Water 2021;13(9):1211.
[12] Lakkaboyana SK, et al. Preparation of novel chitosan polymeric nanocomposite as an efficient material for the removal of Acid Blue 25 from aqueous environment. Int J Biol Macromol 2021;168:760–8.
[13] Jabeen S, et al. Palladium-Supported Zirconia-Based Catalytic Degradation of Rhodamine-B Dye from Wastewater. Water 2021;13(11). https://doi.org/10.3390/w13111522.
[14] Vallinayagam S, et al. Recent developments in magnetic nanoparticles and nano-composites for wastewater treatment. J Environ Chem Eng 2021;9(6):106553.
[15] Anbia M, Ghaffari A. Adsorption of phenolic compounds from aqueous solutions using carbon nanoporous adsorbent coated with polymer. Appl Surf Sci 2009;255(23):9487–92.
[16] Gonte RR, Shelar G, Balasubramanian K. Polymer–agro-waste composites for removal of Congo red dye from wastewater: adsorption isotherms and kinetics. Desalin Water Treat 2014;52(40-42):7797–811.
[17] Liu J, et al. Adsorption of bromophenol blue from aqueous samples by novel supported ionic liquids. J Chem Technol Biotechnol 2014;89(2):230–8.
[18] Dhananasekaran S, Palanivel R, Pappu S. Adsorption of Methylene Blue, Bromophenol Blue, and Coomassie Brilliant Blue by alpha-chitin nanoparticles. J Adv Res 2016;7(1):113–24. https://doi.org/10.1016/j.jare.2015.03.003.
[19] Nayunigari MK, et al. Folic acid modified cross-linked cationic polymer: Synthesis, characterization and application of the removal of Congo red dye from aqueous medium. J Mol Liq 2017;227:87–97.
[20] Sasmal D, et al. Selective adsorption of Pb (II) ions by amylopectin-g-poly (acrylamide-co-acrylic acid): A bio-degradable graft copolymer. Int J Biol Macromol 2017;97:585–97.
[21] Kloster GA, Mosiewicki MA, Marcovich NE. Chitosan/iron oxide nanocomposite films: Effect of the composition and preparation methods on the adsorption of congo red. Carbohydr Polym 2019;221:186–94.
[22] Xu HX, et al. Effect of surface modification on quinoline adsorption onto coking coal. Desalin Water Treat 2019;159:282–9. https://doi.org/10.5004/dwt.2019.24138.
[23] Xu M-Y, et al. Highly efficient selective adsorption of anionic dyes by modified β-cyclodextrin polymers. J Taiwan Inst Chem Eng 2020;108:114–28.
[24] Wahab M, et al. Adsorption-Membrane Hybrid Approach for the Removal of Azithromycin from Water: An Attempt to Minimize Drug Resistance Problem. Water 2021;13(14). https://doi.org/10.3390/w13141969.
[25] Bhaumik M, McCrindle R, Maity A. Efficient removal of Congo red from aqueous solutions by adsorption onto interconnected polypyrrole–polyaniline nanofibres. Chem Eng J 2013;228:506–15.

[26] You L, et al. Facile synthesis of high performance porous magnetic chitosan - polyethylenimine polymer composite for Congo red removal. Int J Biol Macromol 2018;107(Pt B)):1620–8. https://doi.org/10.1016/j.ijbiomac.2017.10.025.
[27] Guo D-D, et al. Ladder chain Cd-based polymer as a highly effective adsorbent for removal of Congo red. Ecotoxicol Environ Saf 2019;178:221–9.
[28] Feng C, et al. Facile synthesis of trimethylammonium grafted cellulose foams with high capacity for selective adsorption of anionic dyes from water. Carbohydr Polym 2020;241:116369.
[29] Kalla RMN, et al. Hierarchically porous polyaromatic carbon spheres decorated $NiMn_2O_4$ nanocomposite: efficient selective azo dye degradation from aqueous water and reduction of p-nitrophenol to p-aminophenol. Carbon Lett 2024. https://doi.org/10.1007/s42823-023-00685-y.
[30] Akpomie KG, Conradie J. Biogenic and chemically synthesized Solanum tuberosum peel-silver nanoparticle hybrid for the ultrasonic aided adsorption of bromophenol blue dye. Sci Rep 2020;10(1):17094. https://doi.org/10.1038/s41598-020-74254-y.
[31] Agency, E.C. Summary of Classification and Labelling. 2024; Available from: https://echa.europa.eu/information-on-chemicals/cl-inventory-database/-/discli/details/107684.
[32] Aygün A, Yenisoy-Karakaş S, Duman I. Production of granular activated carbon from fruit stones and nutshells and evaluation of their physical, chemical and adsorption properties. Microporous Mesoporous Mater 2003;66(2-3):189–95.
[33] Alves DC, et al. Development of Spirulina/chitosan foam adsorbent for phenol adsorption. J Mol Liq 2020;309:113256.
[34] Demissie H, et al. Removal of phenolic contaminants from water by in situ coated surfactant on Keggin-aluminum nanocluster and biodegradation. Chemosphere 2021;269:128692.
[35] Ramires P, Milella E. Biocompatibility of poly (vinyl alcohol)-hyaluronic acid and poly (vinyl alcohol)-gellan membranes crosslinked by glutaraldehyde vapors. J Mater Sci: Mater Med 2002;13(1):119–23.
[36] Migneault I, et al. Glutaraldehyde: behavior in aqueous solution, reaction with proteins, and application to enzyme crosslinking. Biotechniques 2004;37(5):790–802.
[37] Kulkarni VH, Kulkarni PV, Keshavayya J. Glutaraldehyde-crosslinked chitosan beads for controlled release of diclofenac sodium. J Appl Polym Sci 2006;103(1):211–7. https://doi.org/10.1002/app.25161.
[38] Bolto B, et al. Crosslinked poly (vinyl alcohol) membranes. Prog Polym Sci 2009;34(9):969–81.
[39] More SM, et al. Glutaraldehyde-crosslinked poly (vinyl alcohol) hydrogel discs for the controlled release of antidiabetic drug. J Appl Polym Sci 2010;116(3):1732–8.
[40] Martinez AW, et al. Effects of crosslinking on the mechanical properties, drug release and cytocompatibility of protein polymers. Acta Biomater 2014;10(1):26–33.
[41] Li K, et al. Enhancing enzyme activity and enantioselectivity of Burkholderia cepacia lipase via immobilization on melamine-glutaraldehyde dendrimer modified magnetic nanoparticles. Chem Eng J 2018;351:258–68.
[42] de Andrades D, et al. Immobilization and stabilization of different beta-glucosidases using the glutaraldehyde chemistry: Optimal protocol depends on the enzyme. Int J Biol Macromol 2019;129:672–8. https://doi.org/10.1016/j.ijbiomac.2019.02.057.
[43] Gao Y, et al. Physicochemical properties of zein films cross-linked with glutaraldehyde. Polym Bull 2022;79(7):4647–65.
[44] Khan MA, et al. Synthesis and Characterization of Acrylamide/Acrylic Acid Co-Polymers and Glutaraldehyde Crosslinked pH-Sensitive Hydrogels. Gels 2022;8(1):47.
[45] Abellanas-Perez P, et al. Glutaraldehyde modification of lipases immobilized on octyl agarose beads: Roles of the support enzyme loading and chemical amination of the enzyme on the final enzyme features. Int J Biol Macromol 2023;248:125853. https://doi.org/10.1016/j.ijbiomac.2023.125853.
[46] Şenkal BF, Biçak N. Glycidyl methacrylate based polymer resins with diethylene triamine tetra acetic acid functions for efficient removal of Ca (II) and Mg (II). React Funct Polym 2001;49(2):151–7.
[47] Kasgöz H, Özgümüs S, Orbay M. Modified polyacrylamide hydrogels and their application in removal of heavy metal ions. Polymer 2003;44(6):1785–93. https://doi.org/10.1016/s0032-3861(03)00033-8.
[48] Zhang Y, et al. Chemical modification of silica-gel with diethylenetriamine via an end-group protection approach for adsorption to Hg(II). Appl Surf Sci 2009;255(11):5818–26. https://doi.org/10.1016/j.apsusc.2009.01.011.
[49] Wang H, Paul DR, Chung TS. Surface modification of polyimide membranes by diethylenetriamine (DETA) vapor for H_2 purification and moisture effect on gas permeation. J Membr Sci 2013;430:223–33. https://doi.org/10.1016/j.memsci.2012.12.008.
[50] Lavrenyuk H, et al. A new flame retardant on the basis of diethylenetriamine copper (II) sulfate complex for combustibility suppressing of epoxy-amine composites. Fire Saf J 2016;80:30–7. https://doi.org/10.1016/j.firesaf.2016.01.001.
[51] Yang YQ, Chuah CY, Bae TH. Highly efficient carbon dioxide capture in diethylenetriamine-appended porous organic polymers: Investigation of structural variations of chloromethyl monomers. J Ind Eng Chem 2020;88:207–14. https://doi.org/10.1016/j.jiec.2020.04.014.
[52] Hasan N, et al. Diethylenetriamine/NONOate-doped alginate hydrogel with sustained nitric oxide release and minimal toxicity to accelerate healing of MRSA-infected wounds. Carbohydr Polym 2021;270. https://doi.org/10.1016/j.carbpol.2021.118387.
[53] Mohd NH, et al. Aminosilanes grafted nanocrystalline cellulose from oil palm empty fruit bunch aerogel for carbon dioxide capture. J Mater Res Technol-JmrT 2021;13:2287–96. https://doi.org/10.1016/j.jmrt.2021.06.018.
[54] Jiang XC, et al. Facile synthesis of Poly(epichlorohydrin-diethylenetriamine) hydrogel for highly selective diclofenac sodium removal. Sep Purif Technol 2022;283. https://doi.org/10.1016/j.seppur.2021.120215.
[55] Zelenka T, et al. Carbon dioxide and hydrogen adsorption study on surface-modified HKUST-1 with diamine/triamine. Sci Rep 2022;12(1). https://doi.org/10.1038/s41598-022-22273-2.
[56] Gao XP, et al. Photocatalytic degradation of methyl orange by a diethylenetriamine modified chitosan/bentonite composite. React Chem Eng 2023;8(10):2505–21. https://doi.org/10.1039/d3re00220a.
[57] Gokkus K, et al. Amine-functionalised poly (glycidyl methacrylate) hydrogels for Congo red adsorption. J Environ Eng Sci 2023;18(4):204–14. https://doi.org/10.1680/jenes.23.00025.
[58] Alorabi AQ, Hassan MS, Azizi M. Fe_3O_4-CuO-activated carbon composite as an efficient adsorbent for bromophenol blue dye removal from aqueous solutions. Arab J Chem 2020;13(11):8080–91. https://doi.org/10.1016/j.arabjc.2020.09.039.
[59] Nirmala G, et al. Adsorptive removal of phenol using banyan root activated carbon. Chem Eng Commun 2021;208(6):831–42. https://doi.org/10.1080/00986445.2019.1674839.
[60] Pardo L, et al. Influence of the Structure and Experimental Surfaces Modifications of 2:1 Clay Minerals on the Adsorption Properties of Methylene Blue. Minerals 2018;8(8):359. https://doi.org/10.3390/min8080359.
[61] Lütke SF, et al. Preparation of activated carbon from black wattle bark waste and its application for phenol adsorption. J Environ Chem Eng 2019;7(5). https://doi.org/10.1016/j.jece.2019.103396.
[62] Liu MX, et al. Ultrafast and selective adsorption of anionic dyes with amine-functionalized glucose-based adsorbents. J Mol Struct 2022;1263. https://doi.org/10.1016/j.molstruc.2022.133150.
[63] Mhlongo JT, et al. Synthesis and application of cationized cellulose for adsorption of anionic dyes. International Symposium on Nanostructured and Advanced Materials (ISNNAM). Electr Network,; 2021. https://doi.org/10.1016/j.matpr.2022.02.100.
[64] Shahbazi A, Younesi H, Badiei A. Functionalized SBA-15 mesoporous silica by melamine-based dendrimer amines for adsorptive characteristics of Pb(II), Cu(II) and Cd(II) heavy metal ions in batch and fixed bed column. Chem Eng J 2011;168(2):505–18. https://doi.org/10.1016/j.cej.2010.11.053.
[65] Repo E, et al. Heavy metals adsorption by novel EDTA-modified chitosan-silica hybrid materials. J Colloid Interface Sci 2011;358(1):261–7. https://doi.org/10.1016/j.jcis.2011.02.059.
[66] Lagergren S. Theory so-Call Adsorpt soluble Subst 1898.
[67] Ho Y-S, McKay G. Pseudo-second order model for sorption processes. Process Biochem 1999;34(5):451–65. https://doi.org/10.1016/S0032-9592(98)00112-5.
[68] Weber Jr WJ, Morris JC. Kinetics of adsorption on carbon from solution. J Sanit Eng Div 1963;89(2):31–59. https://doi.org/10.1061/JSEDAI.0000430.
[69] Chien S, Clayton W. Application of Elovich equation to the kinetics of phosphate release and sorption in soils. Soil Sci Soc Am J 1980;44(2):265–8. https://doi.org/10.2136/sssaj1980.03615995004400020013x.
[70] Juang RS, Wu FC, Tseng RL. Mechanism of adsorption of dyes and phenols from water using activated carbons prepared from plum kernels. J Colloid Interface Sci 2000;227(2):437–44. https://doi.org/10.1006/jcis.2000.6912.
[71] Mohanty K, Das D, Biswas MN. Adsorption of phenol from aqueous solutions using activated carbons prepared from Tectona grandis sawdust by $ZnCl_2$ activation. Chem Eng J 2005;115(1-2):121–31. https://doi.org/10.1016/j.cej.2005.09.016.
[72] Coughlin RW, Ezra FS. Role of surface acidity in the adsorption of organic pollutants on the surface of carbon. Environ Sci Technol 1968;2(4):291–7.
[73] Liu J, et al. Adsorption of bromophenol blue from aqueous samples by novel supported ionic liquids. J Chem Technol Biotechnol 2013;89(2):230–8. https://doi.org/10.1002/jctb.4106.
[74] You LJ, et al. Kinetics and thermodynamics of bromophenol blue adsorption by a mesoporous hybrid gel derived from tetraethoxysilane and bis(trimethoxysilyl) hexane. J Colloid Interface Sci 2006;300(2):526–35. https://doi.org/10.1016/j.jcis.2006.04.039.
[75] Djebbar M, et al. Adsorption of phenol on natural clay. Appl Water Sci 2012;2(2):77–86. https://doi.org/10.1007/s13201-012-0031-8.
[76] Es'haghi Z, Vafaeinezhad F, Hooshmand S. Green synthesis of magnetic iron nanoparticles coated by olive oil and verifying its efficiency in extraction of nickel from environmental samples via UV–vis spectrophotometry. Process Saf Environ Prot 2016;102:403–9. https://doi.org/10.1016/j.psep.2016.04.011.
[77] Langmuir I. The constitution and fundamental properties of solids and liquids. Part I. Solids. J Am Chem Soc 1916;38(11):2221–95.
[78] Freundlich HMF. Over the adsorption in solution. J Phys Chem 1906;57(385471):1100–7.
[79] Tempkin M, Pyzhev V. Kinetics of ammonia synthesis on promoted iron catalyst. Acta Phys Chim USSR 1940;12(1):327.
[80] Radushkevich M. The equation of the characteristic curve of the activated charcoal USSR. Phys Chem Sect 1947;55:331.
[81] Sridar R, Ramanane UU, Rajasimman M. ZnO nanoparticles–Synthesis, characterization and its application for phenol removal from synthetic and pharmaceutical industry wastewater. Environ Nanotechnol, Monit Manag 2018;10:388–93. https://doi.org/10.1016/j.enmm.2018.09.003.
[82] Aliabadi M, et al. Electrospun nanofiber membrane of PEO/Chitosan for the adsorption of nickel, cadmium, lead and copper ions from aqueous solution. Chem Eng J 2013;220:237–43. https://doi.org/10.1016/j.cej.2013.01.021.
[83] Sun CL, Wang CS. Estimation on the intramolecular hydrogen-bonding energies in proteins and peptides by the analytic potential energy function. J Mol Struct-Theochem 2010;956(1-3):38–43. https://doi.org/10.1016/j.theochem.2010.06.020.

[84] Yang GD, et al. Simultaneous removal of lead and phenol contamination from water by nitrogen-functionalized magnetic ordered mesoporous carbon. Chem Eng J 2015;259:854–64. https://doi.org/10.1016/j.cej.2014.08.081.
[85] Fseha YH, Shaheen J, Sizirici B. Phenol contaminated municipal wastewater treatment using date palm frond biochar: Optimization using response surface methodology. Emerg Contam 2023;9(1). https://doi.org/10.1016/j.emcon.2022.100202.
[86] Morones-Esquivel MM, et al. Bacterial Communities in Effluents Rich in Phenol and Their Potential in Bioremediation: Kinetic Modeling. Int J Environ Res Public Health 2022;19(21). https://doi.org/10.3390/ijerph192114222.
[87] Shair AS, Dena ASA, El-Sherbiny IM. Matrix-dispersed PEI-coated SPIONs for fast and efficient removal of anionic dyes from textile wastewater samples: Applications to triphenylmethanes. Spectrochim Acta Part a-Mol Biomol Spectrosc 2021;249. https://doi.org/10.1016/j.saa.2020.119301.
[88] Chabalala MB, et al. Mechanistic aspects for the enhanced adsorption of bromophenol blue and atrazine over cyclodextrin modified polyacrylonitrile nanofiber membranes. Chem Eng Res Des 2021;169:19–32.
[89] El-Zahhar AA, Awwad NS, El-Katori EE. Removal of bromophenol blue dye from industrial waste water by synthesizing polymer-clay composite. J Mol Liq 2014;199:454–61.
[90] Saad H, et al. Removal of bromophenol blue from polluted water using a novel azo-functionalized magnetic nano-adsorbent. Rsc Adv 2024;14(2):1316–29. https://doi.org/10.1039/d3ra04222g.
[91] Rastgordani M, Zolgharnein J, Mahdavi V. Derivative spectrophotometry and multivariate optimization for simultaneous removal of Titan yellow and Bromophenol blue dyes using polyaniline@SiO_2 nanocomposite. Microchem J 2020;155. https://doi.org/10.1016/j.microc.2020.104717.
[92] Zhang JC, et al. Porous carbon nanospheres aerogel based molecularly imprinted polymer for efficient phenol adsorption and removal from wastewater. Sep Purif Technol 2021;274. https://doi.org/10.1016/j.seppur.2021.119029.
[93] Cao YW, et al. Acylamino-functionalized hyper-cross-linked polymers for efficient adsorption removal of phenol in aqueous solution. Sep Purif Technol 2022;303. https://doi.org/10.1016/j.seppur.2022.122229.
[94] Zhang JJ, et al. Hydroxyl-functionalized hypercrosslinked polymers with ultrafast adsorption rate as an efficient adsorbent for phenol removal. Microporous Mesoporous Mater 2022;336. https://doi.org/10.1016/j.micromeso.2022.111836.
[95] Wang Y, et al. Acetamido-functionalized hyper-crosslinked polymers for efficient removal of phenol in aqueous solution. Sep Purif Technol 2022;287. https://doi.org/10.1016/j.seppur.2022.120566.
[96] Hao AP, Fu ZY, Huang JH. Acrylate-functionalized hyper-cross-linked polymers: Effect of the porogens in the polymerization on their porosity and adsorption from aqueous solution. Sep Purif Technol 2023;311. https://doi.org/10.1016/j.seppur.2023.123380.
[97] Nakhjiri MT, Marandi GB, Kurdtabar M. Preparation of magnetic double network nanocomposite hydrogel for adsorption of phenol and p-nitrophenol from aqueous solution. J Environ Chem Eng 2021;9(2). https://doi.org/10.1016/j.jece.2021.105039.